THz VNA from AB Millimetre

Especially the 660-1000 GHz WR-1.2 band and the 210-336 GHz WR-3.4 band, including the summary of all other bands
2010 March 1

Philippe Goy, Aleksander Wittlin, AB MILLIMETRE
abmillimetre@wanadoo.fr
www.abmillimetre.com

I. INTRODUCTION.

Thanks to an original patented configuration, the AB MILLIMETRE Company, founded in 1988, opened the possibility of vector measurements at millimeter-submillimeter frequencies, with its Millimeter Vector Network Analyzer model MVNA-8-350. Different setups, all solid-state electronics, have allowed vector measurements up to 1000 GHz for more than ten years.

However, until recently, the Local Oscillators (LOs) for the extensions to the submillimeter domain required mechanically tunable Gunn oscillators. The best Gunn diodes were delivering tens of mW in the extended W frequency band, from 69 to 112 GHz. The drawbacks of these LOs were the necessary delicate PLL controls and the very limited span of electronically driven frequency sweeps.

A few years ago a new, improved technique made it possible to deliver tens of mW in the millimeter extended W-band, from 62 to 112 GHz, with wide W-band active sextuplers. Therefore, Gunn oscillators could be replaced by these fully sweepable LOs.

In AB Millimetre, former Gunn-based submillimeter extensions, called ESA-1 (source) and ESA-2 (detection) are now replaced by the ASA-1 and ASA-2 cascade extensions (An upgrade of MVNAs to such ASA extensions, which are compatible with earlier delivered hardware and software is highly recommended) . The frequency coverage of the source ASA-1 is 140-1000 GHz, and the frequency coverage of the detection unit ASA-2 is 250-1000 GHz. The span of electronically controlled sweeps is of the range of 10 to 20 GHz, and there is no need of any delicate PLL control.

In the recent years there is also a considerable improvement of the Schottky diode technology. New generation diodes are used at the source side (for better multipliers) and on the detection side (for better mixers and harmonic mixers) and we have now much more sensitive detectors for the bands above 130 GHz. Therefore, in parallel with our multi-harmonic multipliers and mixers (extensions ASA-1 and ASA-2), we develop the new multiplication chains covering entire frequency bands without necessity of mechanical tunings.

In this paper we illustrate our state-of-the-art achievements in the 2010, focusing on the introduction of the instrumentation for the full-sweep THz band 660-1000 GHz, with dynamic range approaching 80 dB.

II. DESCRIPTION OF THE SOURCES.

II.1. The THz, WR-1.2 source (660-1000 GHz).

The Source HG-wr1.2-FB covers the 660-1000 GHz frequency interval by multiplying (N=54) the 12.2-18.5 GHz interval coming from the MVNA HG cable, see Fig.1.

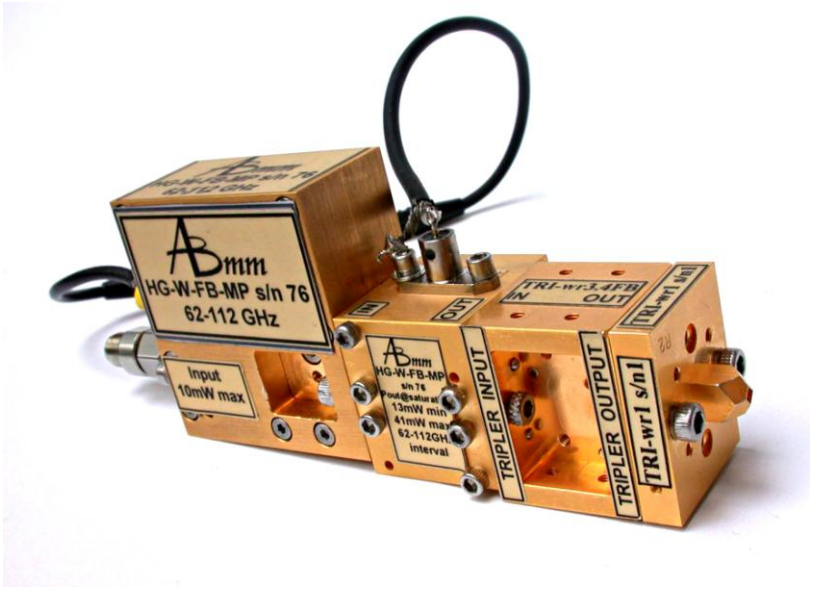

Figure 1. The sub-terahertz submillimeter wave source HG-wr1.2-FB-DH

There is an active sextupler HG-W-FB-MP. The 73-111 GHz power above 10 mW feeds a wide-band tripler TRI-wr3.4-FB, with a WR-3.4 waveguide output. It provides a spectral range of 220-333 GHz with output power of ca 1 mW, which feeds the input of the last wide-band tripler TRI-wr1.2-FB producing 660-1000 GHz output. This last tripler is terminated with a waveguide WR-1.2, or with a diagonal horn DH, then named TRI-wr1.2-FB-DH, like shown above.

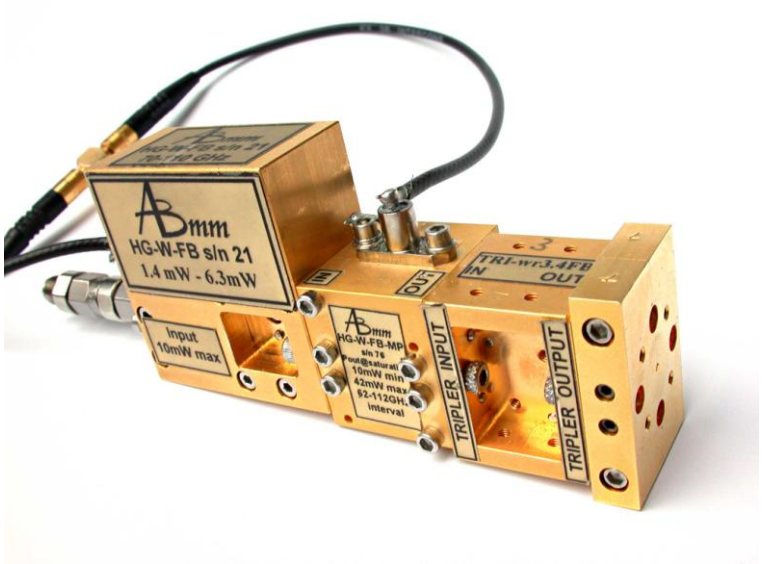

Figure 2. The sub-terahertz submillimeter wave source HG-wr1.2-FB shown in the version furnished with TRI-wr1.2-FB tripler.

II.2. The WR-3.4 source (210-336 GHz).

It is obvious that, when the last tripler HG-wr1.2-FB (Fig.3) is removed, the remaining setup called HG-wr3.4-FB can be used as a source itself. In other words, the 220-336 GHz WR-3.4 band source is a kind of by-product of the THz source. Actually, it is also the case of the 62-112 GHz HG-W-FB-MP extended W-band source after removing the tripler TRI-wr3.4-FB (Fig. 3).

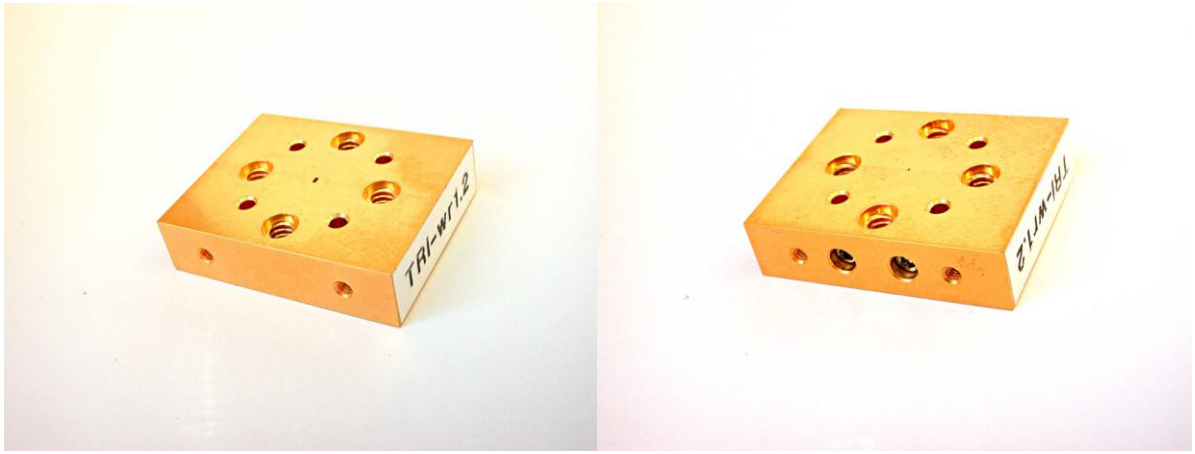

Figure 3. Tripler TR1-wr1.2-FB. Left picture – input side with WR-3 waveguide for 220-330 GHz, 0.1 – 1 mW input signal. Right picture - output side with WR-1.2 providing 1-10 microwatts at 660-1000 GHz.

See the respective powers of this 210-340 GHz HG-wr3.4-FB source Fig.4A, and of the 660-1000 GHz source HG-wr1.2-FB, Fig.4B. Comparing the input/output power levels, the first tripler TRI-wr3.4-FB has a maximum efficiency of approx. 3%, and the second tripler TRI-wr1.2-FB of approx. 1%.

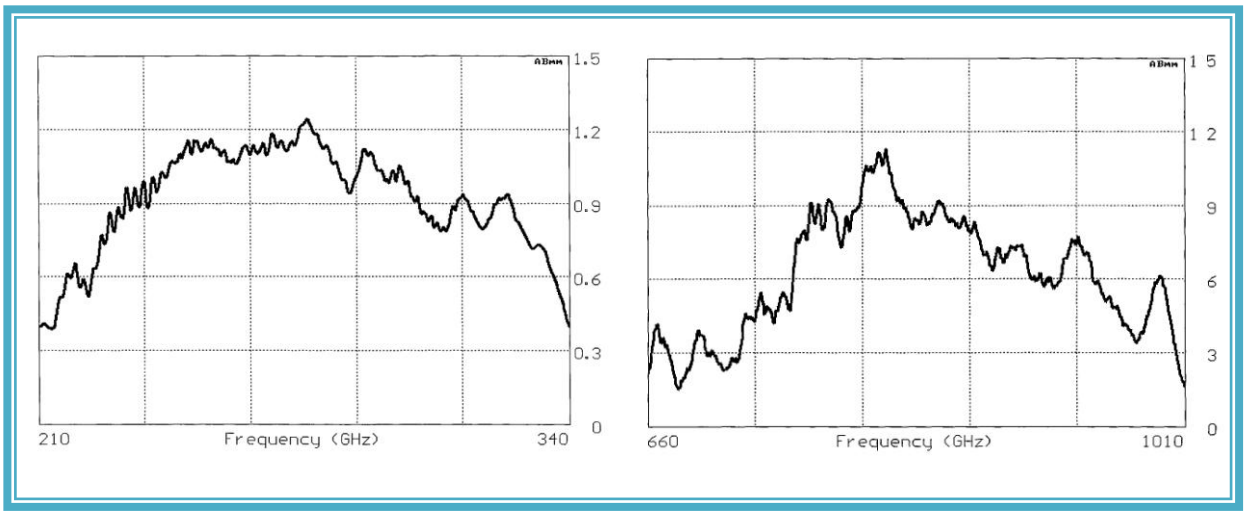

Figure 4. Typical output power shown in milliwatts over the spectral range 210-340 GHz as measured for the HG-wr3.4-FB source (left panel) and a typical output power, shown in microwatts over the spectral range 660-1010 GHz for the HG-wr1.2-FB source (right panel).

II.3. Precision control of emitted power in the 660-1000 GHz spectral range.

Calibrated W-band rotary vane attenuator located between the LO W-band source and the 1st Tripler (Fig.5), allows to reduce the power emitted by the mutiplication chain to a level as low as desired.

Figure 5. Regulated output power sub-terahertz radiation source.

The dependence of the output signal on the input power at a fixed frequency 969 GHz, Fig.6, shows that the multiplication chain is close to saturation (the slope is 1dB/dB) at maximum applied power, and that the desaturation occurs rapidly, ca -3 dB on the rotary-vane attenuator.

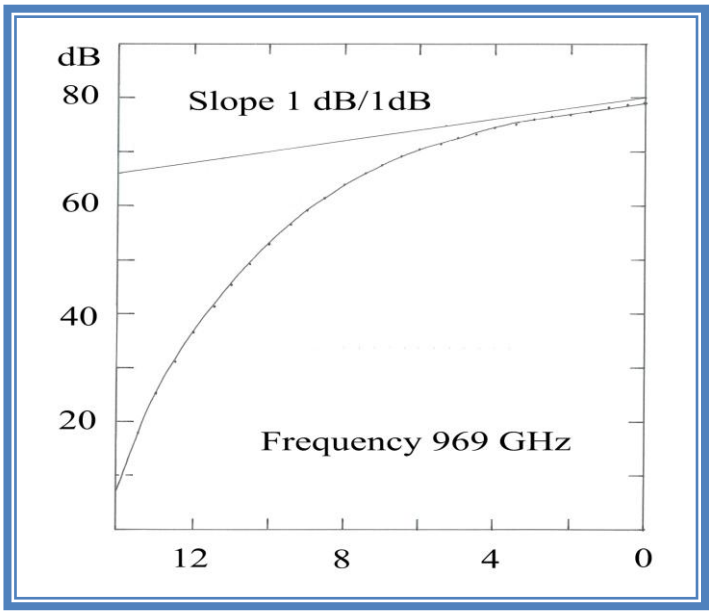

Figure 6. The output power of the MVNA (in dB, arbitrary scale) versus rotary vane attenuator position (in dB).

The large dynamic range of the MVNA allows to evaluate powers down to the pW level, corresponding to approx. 10 dB in the arbitrary dB vertical scale of Fig. 6 by comparison with

the maximum power obtained from an absolute power meter (calorimeter), as shown in Fig.4B.

III. DESCRIPTION OF THE DETECTION.

III.1. HM-wr3.4 detector for the band 220-336 GHz.

It is a tunable detector with WR-3.4 waveguide, round flange UG-387/U Mod anti-cocking input, Fig.7.

Figure 7. Tunable detector HM-wr3.4.

Its frequency response versus a rather flat power presents structures, the position of which depends on the position of the tuning short, see Fig.8A.

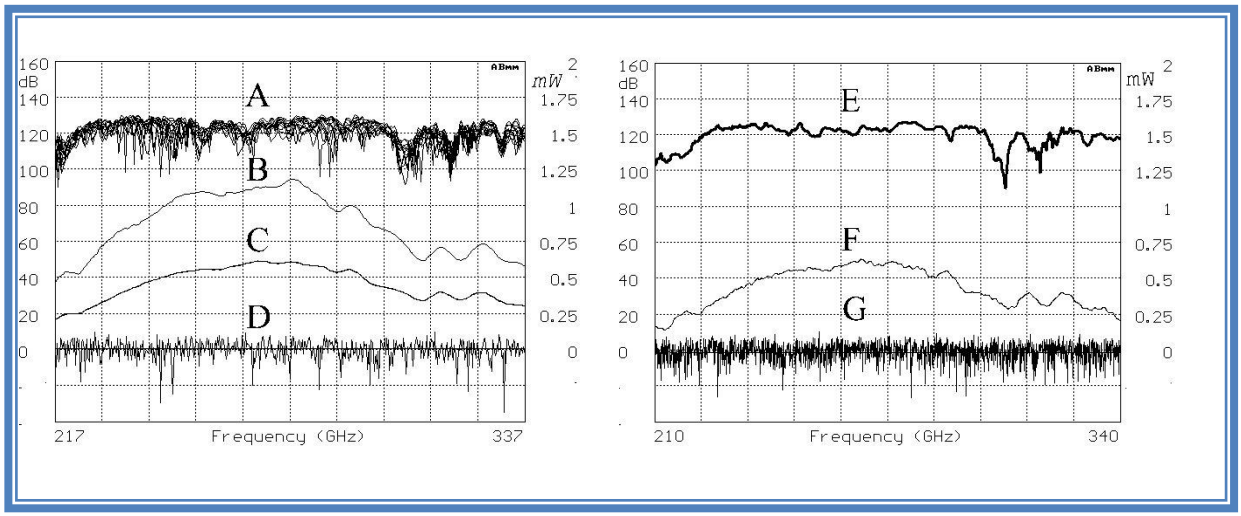

Figure 8. The dynamic range (DR – in dB, left scale) versus frequency of the tunable detector HM-wr3.4. On the left plot (Fig. 8A) the DR is shown in trace A for several different positions of the tuning short. The power delivered by the source HG-wr3.4-FB is shown as B (right scale in mW), and the power across the directional coupler DC (used for stimultaneous measurements of the DR and P - the measured power), reduced by the insertion loss (ca 3 dB) of the DC is shown as trace C. The lowest trace D shows the noise floor of the detector. On the right plot (Fig. 8B) the uppermost trace E shows the DR after removing the tunable short. The trace F shows the power across the directional coupler (analogous to C in the left plot), and the trace G shows the noise level.

In case one removes the tuning short as indicated Fig.7, the frequency response becomes reasonably flat, see Fig.8B.

III.2. ASA-2 extension to detect above 250 GHz.

See Fig.9. This extension uses a mechanically-tunable multi-harmonic mixer, and has the capability to detect any frequency above its input cutoff at 250 GHz. In the Fig.9 it is equipped, at its input, by the flange with WR-2.8 waveguide for the range 250-400 GHz with the waveguide cutoff at 211 GHz. A transition to WR-3.4 permits a very sensitive detection of HG-wr3.4-FB (Dynamic range DR ca 130 dB in the frequency range 250-336 GHz.).

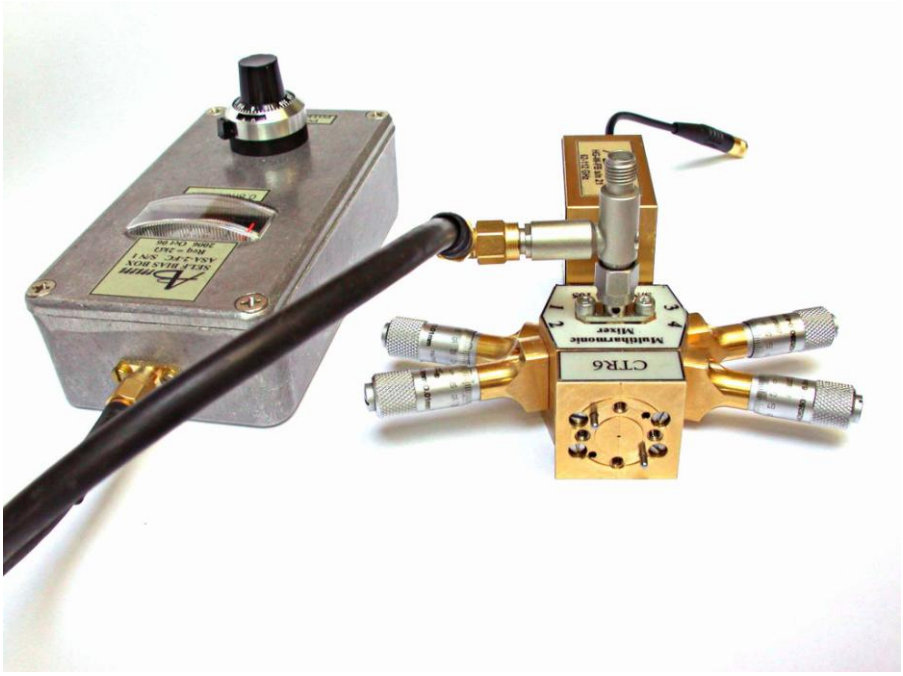

Figure 9. The ASA-2-FC extension for signal detection at 250-1000 GHz . Upon mechanical tuning to the central frequency desired the typical electronically-tuned sweep spans over 10-20 GHz.

With a WR-1.2 input it can detect the HG-wr1.2-FB THz source. However the frequency sweep spans are limited to, typically, 20 GHz.

III.3. The HM-wr1.2-FB wide-band, sensitive, full-sweep detector.

See Fig.10. A sensitive harmonic mixer is fed, through an isolator, by its LO. At top of the mixer is a bias tee for separation of the DC from the IF out of the mixer.

Figure 10. The full-band (not tuned) detector HM-wr1.2-FB for the sub-teraherz spectral range 660-1000 GHz.

The Fig.11 shows the input flange, WR-1.2 waveguide, round flange UG-387/U Mod anti-cocking, of the detector HM-wr1.2-FB.

Figure 11. Detail picture of the HM-wr1.2-FB input round flange UG387/U Mod anti-cocking waveguide WR-1.2

Fig.12 shows this input equipped with a Scalar Horn for free space detection of the 660-1000 GHz band.

Figure 12. Detail picture of the HM-wr1.2-FB detector head equipped with a scalar (corrugated) horn.

Fig.13 shows this input equipped with a diagonal horn DH-wr1.2 for the 660-1000 GHz band.

Figure 13. HM-wr1.2-FB input equipped with a diagonal horn.

The detections of the HG-wr1.2-FB source by the extension ASA-2, operated after many mechanical tunings, for limited frequency sweep spans are shown in Fig. 14A. In Fig.14B, we show a spectrum of a single sweep with a nearly constant response with DR ca 80 dB obtained with the Flat Broadband FB detector HM-wr1.2-FB. This last detector is much more easy and quick to use then the ASA-2-FC detection in the range 660-1000 GHz.

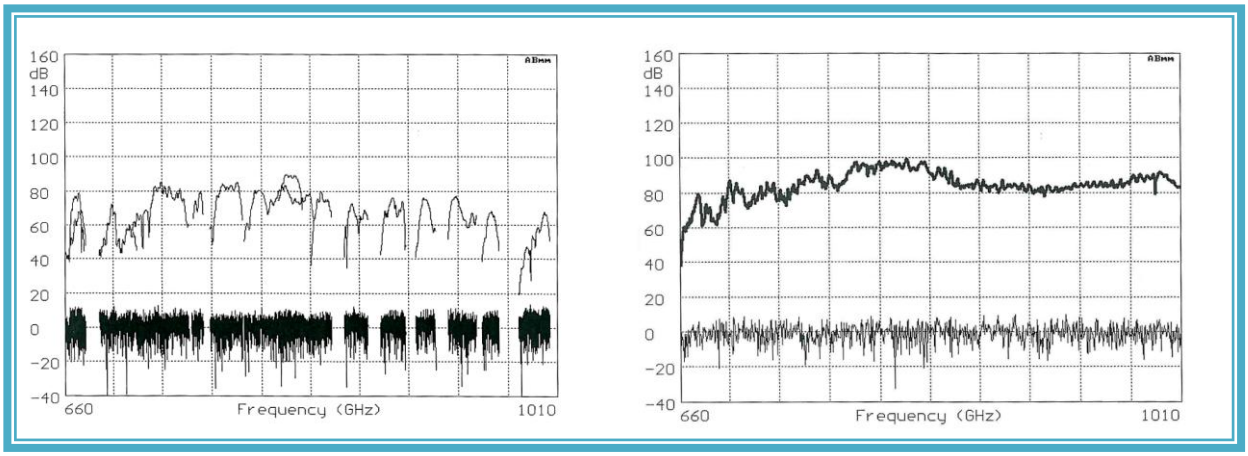

Figure 14. The dynamic range of the setup composed of the HG-wr1.2-FB source (see Fig.1,2) and of the extension ASA-2-FC detector (see Fig.9) is shown on the left picture (Fig. 14A). The right picture (Fig. 14B) demonstrates nearly flat dynamic response of the setup of the same source HG-wr1.2-FB with the Flat Broadband detector HM-wr1.2-FB (see Fig.10).

IV. SPECIFICATION OF THE AB MILLIMETRE's MVNA-8-350 (2010)

IV.1. The available CW power.

Fig.15 gives the typical power in all cases, see Table 1, from Q-band, starting at 29 GHz, line (a). The power at frequencies below, from 8 GHz (our absolute lower limit) to 29 GHz, is larger.

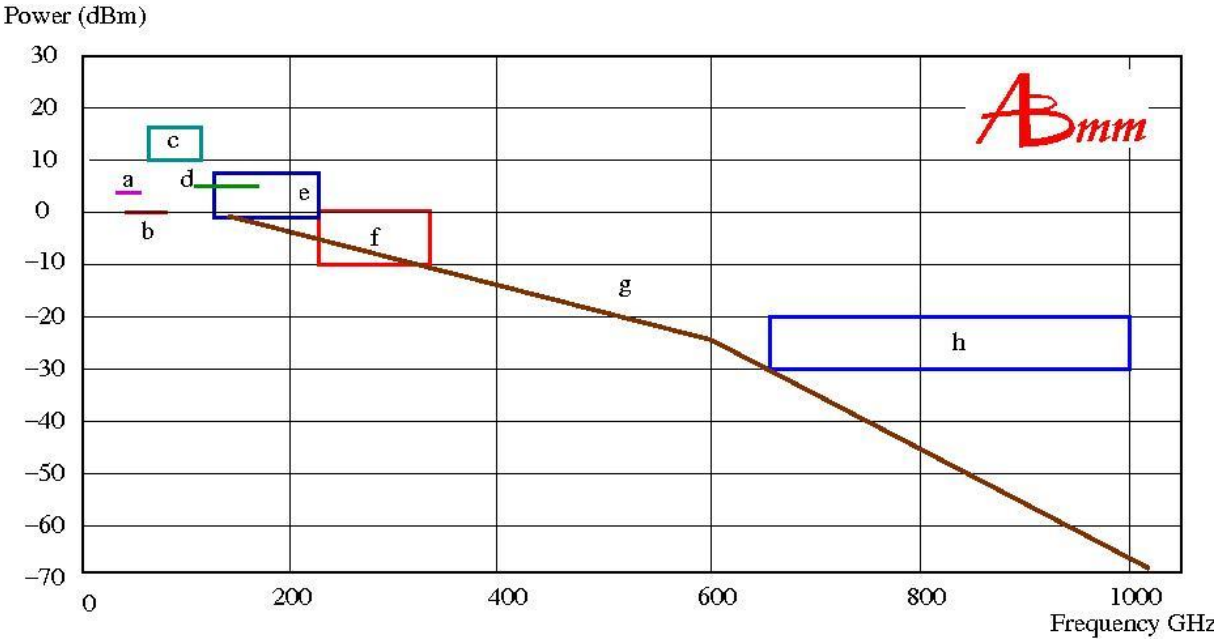

Figure 15. The output power of sources of MVNA over the whole spectrum. The symbols are explained in the Table 1 below.

The square (c) is the HG-W-FB-MP, the square (e) is HG-W-FB-MP feeding a doubler DOU-wr5.1-FB (band 130-224 GHz). The square (f) is the source HG-wr3.4-FB, in other words the HG-W-FB-MP feeding the Tripler TRI-wr3.4-FB. The square (h) is HG-wr1.2-FB (II.1), Figs.1-2, which is source HG-wr3.4-FB feeding the last tripler TRI-wr1.2-FB. The brown line (g) is the power delivered by the extension ASA-1, after its mechanical tunings.

Table 1				
Submillimeter sources from AB Millimetre				
	Source	**Frequency band**	**Waveguide**	**Power (typical)**
	Catalog type	*GHz*		mW
a	HG-Q-FB	29-51	WR-22	1-5
b	HG-V-FB	44-75	WR-15	≤ 1
c	HG-W-FB-MP	62-112	WR-10	8-40
d	HG-D-FB	110-170	WR-6.5	1-9
e	HG-wr5.1-FB	130-224	WR-5.1	0.2-5
f	HG-wr3.4-FB	220-336	WR-3.4	0.1-1
g	ASA-1-FC	140-220	WR-5.1	0.3-0.7
g	ASA-1-FC	220-336	WR-3.4	0.06-0.3
g	ASA-1-FC	260-400	WR-2.8	0.03-0.2
g	ASA-1-FC	400-660	WR-1.9	10^{-3}-$3*10^{-2}$
h	HG-wr1.2-FB	660-1000	WR-1.2	10^{-3}-10^{-2}

IV.2. The available dynamic range DR.

Fig.16 gives the typical DR in all cases from Q-band (starting at 29 GHz, a). DRs at frequencies below, from 8 GHz (our absolute lower limit) to 29 GHz are the same, or larger.

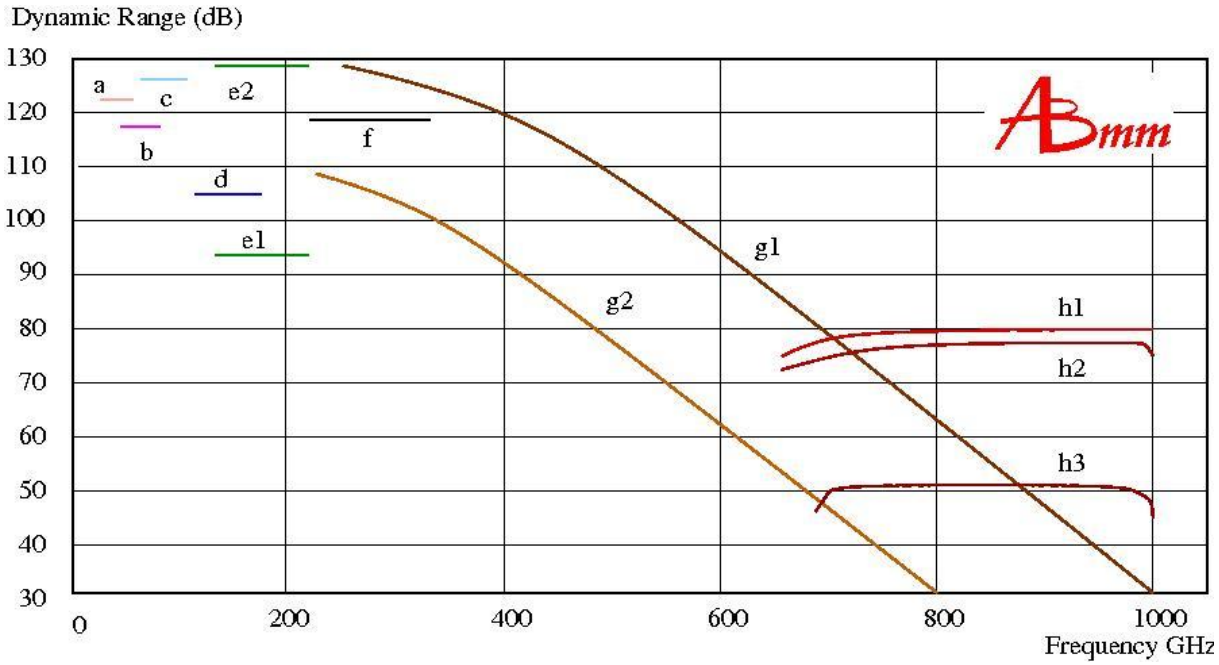

Figure 16. The dynamic range of MVNA over the whole spectral range. The symbols are explained in the Table 2 below.

Table 2				
Dynamic range of MVNA-8-350 with different sources and detectors				
	Source	**Frequency band**	**Waveguide**	**Detector**
	Catalog	*GHz*		*Catalog*
a	HG-Q-FB	29-51	WR-22	HM-Q-FB
b	HG-V-FB	44-75	WR-15	HM-V-FB
c	HG-W-FB-MP	62-112	WR-10	HM-W-FB
d	HG-D-FB	110-170	WR-6.5	HM-D-FB
e1	HG-wr5.1-FB	130-224	WR-5.1	HM-D-FB*
e2	HG-wr5.1-FB	130-224	WR-5.1	HM-wr5.1**
f	HG-wr3.4-FB	220-336	WR-3.4	HM-wr3.4**
g1	ASA-1-FC	250-800	WR-5.1/1.9	ASA-2-FC***
g2	ASA-1-FC	220-800	WR-5.1/1.9	HM-wr3.4***
h1	HG-wr1.2-FB	660-1000	WR-1.2	HM-wr1.2-FB
h2	HG-wr1.2-FB	660-1000	WR-1.2	ASA-2-FC***
h3	HG-wr1.2-FB	660-1000	WR-1.2	HM-wr3.4***
**detector attached through transition RT-wr6.5/wr5.1*				
***mechanically tunable detector head*				
****electronically tunable frequency span approx. 20 GHz*				

Additional notes to the Fig. 16 and Table 2 are given on the next page.

(e1)-(e2) In the case of the source HG-wr5.1-FB, there are two possible detectors: the non-tunable HM-D-FB, which gives rather flat response with frequency (DR ca 90 dB) and the tunable HM-wr5.1, much more sensitive (by >25 dB), however giving strong structures with frequency.
(f), see (E) Fig.8B, is the source HG-wr3.4-FB detected by HM-wr3.4 (Fig.7).
(h1), see Fig.14B, is the source HG-wr1.2-FB (Figs.1-2) detected by HM-wr1.2-FB (Fig.10).
(h2), see Fig.14A, is the source HG-wr1.2-FB (Figs.1-2) detected by ASA-2-FC (Fig.9).
(h3) is the source HG-wr1.2-FB (Figs.1-2) detected by HM-wr3.4 (Fig.7).

V. EXAMPLES OF USE OF THESE BANDS FOR DIELECTRICS CHARACTERIZATION.

V.1. The 5-mirror QO bench.

For high sensitivity broad band characterization of dielectrics, ferrites, dispersive metamaterials etc. AB Millimetre developed a sophisticated 5-mirror Reflection/Transmission bench covering full spectral range 44-1000 GHz, shown below.

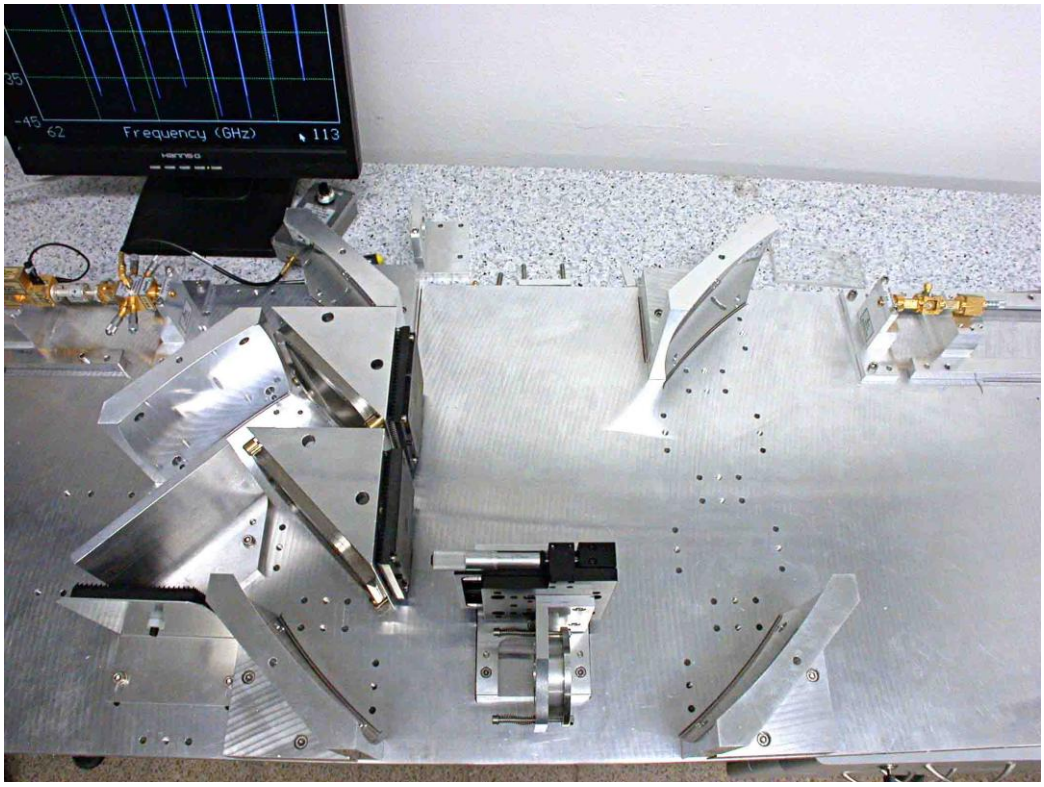

Figure 17. Broadband 44-1000 GHz five-mirror R/T optical bench of AB Millimetre. The two polarizing grids on the source side (mounted on triangles seen on the left side) play very efficiently the role of directional coupler and isolator in the whole 44-1000 GHz spectral range.

V.2. The 2-lens QO setup.

In the following our reflection/transmission quasi-optical R/T QO setup is a very simple two-lens bench, as shown in Fig.18. The T calibration is made with empty sample's place. The R calibration is made with a metal mirror instead of the sample.
R measurements are limited to the availability of directional couplers attached to the horn on the source side (<336 GHz in our case).

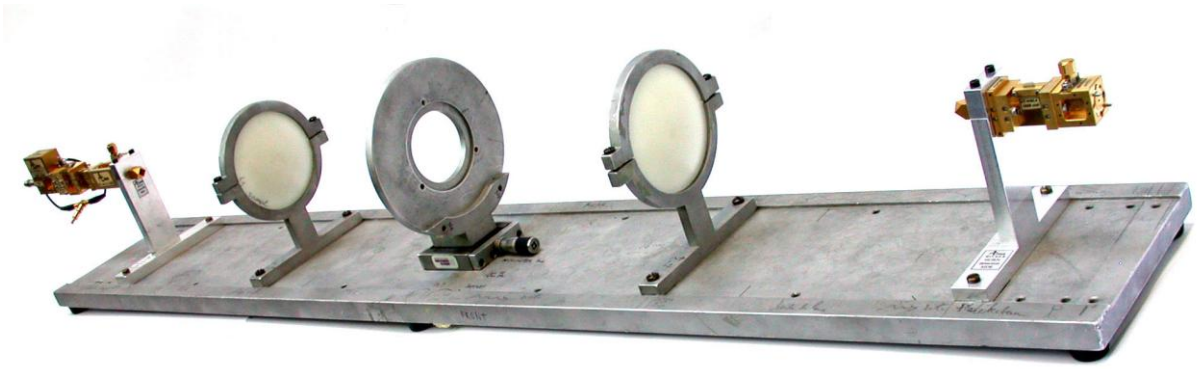

Figure 18. The QO bench with two lenses for transmission measurements. The bench works from 44 GHz (the diffraction limit determined by the size of lenses) up to above 1 THz, where absorption in lenses might limit the dynamic range. For reflectivity measurements the bench works and from 44 GHz to 336 GHz. The upper boundary being limited by performance of available directional couplers.

Fig.19 shows details of the source side in 210-336 GHz WR-3.4 R/T experiments.

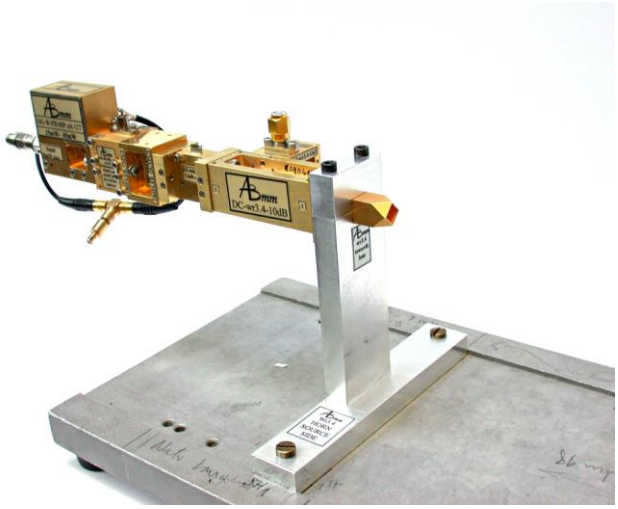

Figure 19. The HG-wr3.4-FB source is attached to the directional coupler DC-wr3.4-10dB, together with the HM-wr3.4 detector (behind the coupler) for the reflectivity measurements. The set-up, with transmitting/receiving horn is mounted on the axis of the QO bench.

Fig.20 shows the detection side for transmission measurements on the quasi-optical bench at the spectral range 210-336 GHz with the HM-wr3.4 detector.

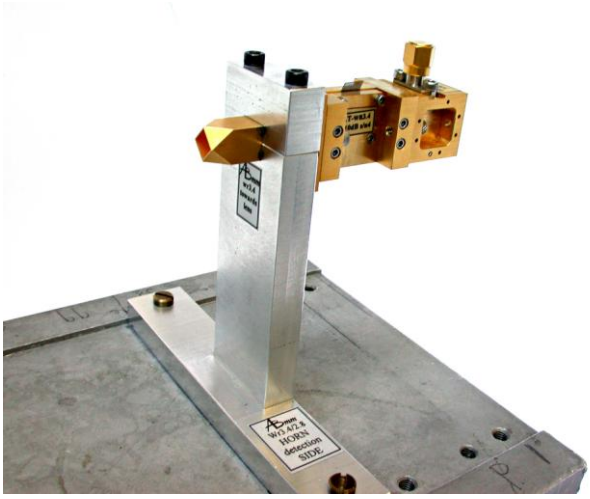

Figure 20. Detector HM-wr3.4, with diagonal horn DH-wr3.4 mounted on the QO bench.

For transmission measurements at the spectral range 660-1000 GHz, the setup is similar, with diagonal horns DH-wr1.2 used instead of the DH-wr3.4.

V.3. Measurements in the 210-336 GHz band.

Figs.21 show the quality of R/T measurements of a very low-loss material, a 1.98 mm thick slab of intrinsic silicon. There is a special software for the fitting of dielectric materials slabs. The permittivity ε is calculated from the phase variation and from the periodicity of the sample behaving as a Fabry-Perot resonator. The value of loss tangent tan δ is extremely small, but it is visible since the maximum transmission peaks do not reach exactly 0 dB. Since it is very small, the uncertainty on it is large.

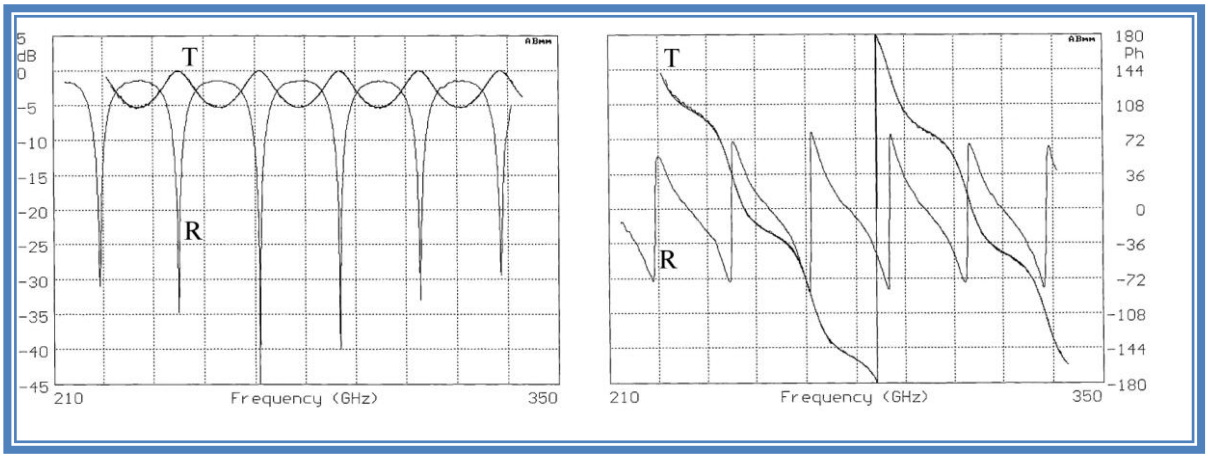

Figure 21. The amplitude (left figure) and the phase (right figure) of signals transmitted through "T", and reflected from "R" a 1.98 mm thick silicon slab between 210 and 336 GHz.

Both T and R spectra show characteristic standing-wave resonances in the plane-parallel sample. The (frequency independent) dielectric constant obtained from the model fit to the experimental data is $\varepsilon = 11.607$, and the loss tangent is $\tan\delta = 0.00017$.
Fig.22 shows the result of a similar experiment of transmission through a low-loss sapphire sample. It is not easy to distinguish the experimental trace (thin) from the theoretical fit (thick). In the polar plot shown in the right of Fig.22, the small discrepancies between the

experiment and the fit are better visible. The absolute accuracy of determination of the dielectric constant is limited by the accuracy of sample thickness measurements.

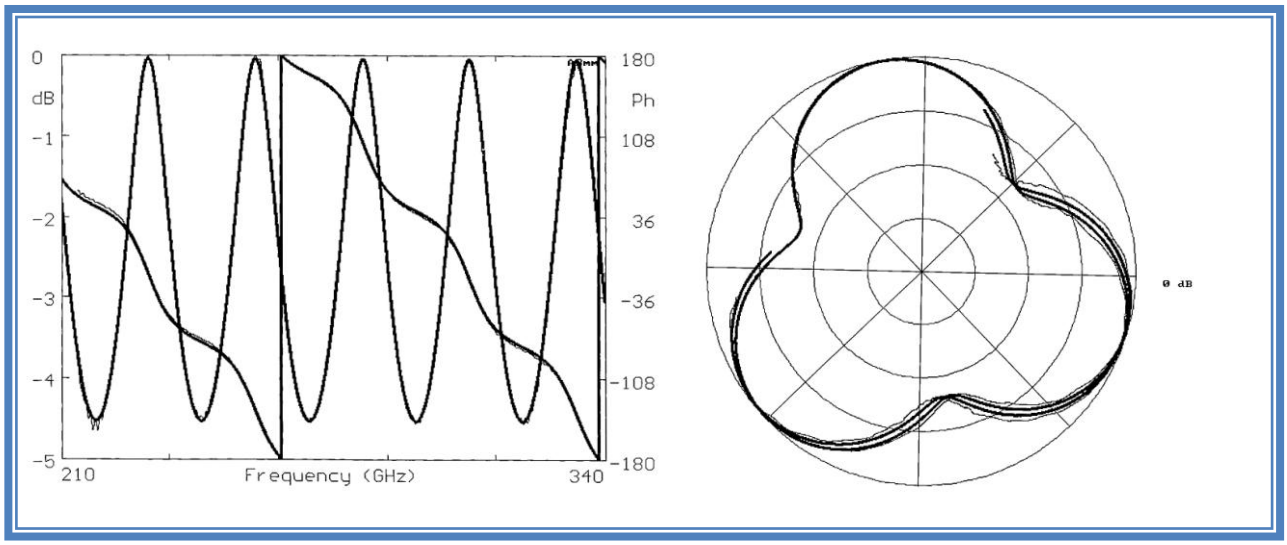

Figure 22. The left picture shows the amplitude (in dB) and the phase (in degrees) of signals transmitted through a 1.916 mm thick sapphire slab between 210 and 336 GHz. Transmission spectra show characteristic for plane-parallel low-losses slabs standing-wave resonances. The (frequency independent) dielectric constant obtained from the model fit to the experimental data is $\varepsilon = 9.371$, and the loss tangent is $\tan\delta = 0.0002$. The right picture shows the same data (thin line) together with the fit (thick line) drawn in the polar coordinates.

V.4. Measurements in the 660-1000 GHz band (transmission).

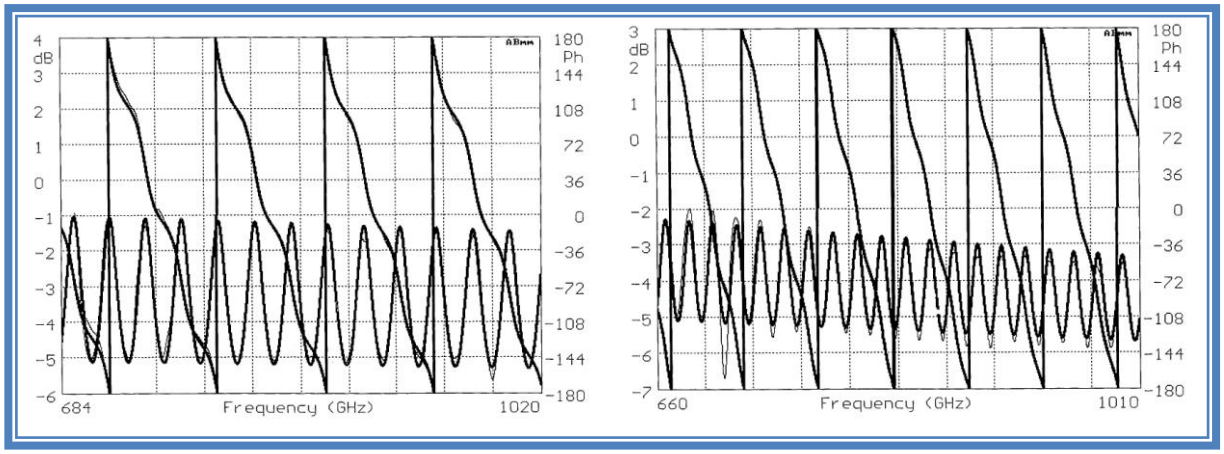

Figure 23. Transmission measurements through the 1.916 mm thick sapphire slice (left plot) and 3 mm thick $MgAl_2O_4$ oxide ceramics (right plot) over the spectral range 660-1020 GHz. Both, the amplitude (in dB, left scale) and the phase (in degrees, right scale) measurements are shown. The dielectric constant ε and loss tangent $\tan\delta$ are 9.441 and 0.00166 for sapphire, and 8.191 and 0.0030 for the ceramics.

Fig.23 shows a transmission through the same sapphire sample as in Fig.22. The transmission maxima are far below 0 dB. The calculated sample loss is $\tan\delta = 0.0017$, and it is

significantly larger than that of 0.0002 previously obtained at lower frequencies, as shown in Fig.22. Fig.23 (right plot) shows also a transmission through a ceramic material with a relatively small loss, with the loss tangent tan δ of the order of 10^{-4} at 100 GHz. Decrease of signal intensity at higher frequencies indicates that the sample becomes lossy (tan δ = 0.003) close to THz frequencies.

V.5. Measurements in the two bands 210-336 and 660-1000 GHz.

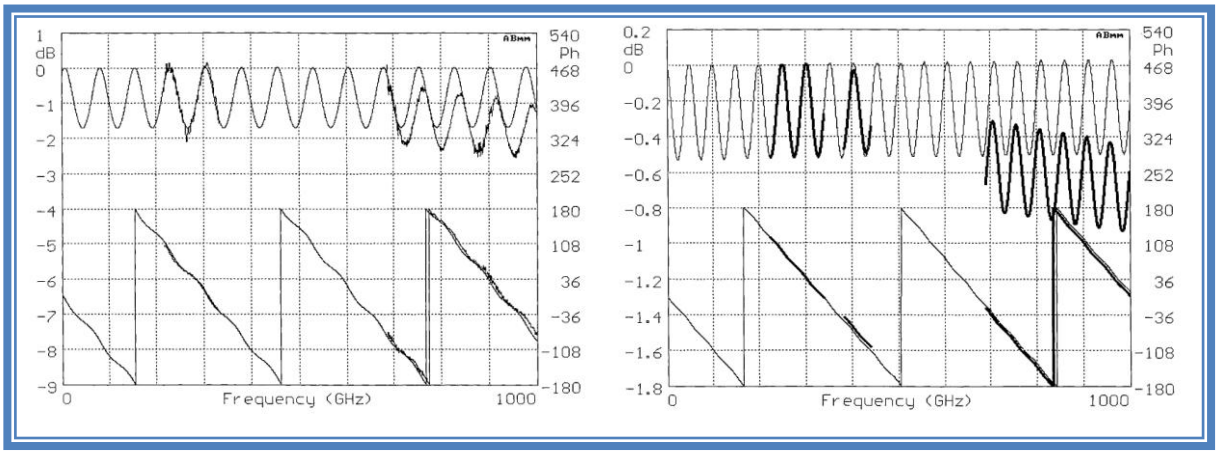

Figure 24. Measured, and extrapolated for the whole spectral range from 0 to 1000 GHz, transmission spectra of silica (left) and Teflon (right) slabs. Upper traces show transmission amplitude (in dB, left scale), bottom traces show transmission phase variations (in degrees, right scale).

In Fig.24 the left picture shows the fit of the experimental trace of transmission of the silica slab in the "low" (210-336 GHz) frequency band which is extrapolated to the interval 0-1000 GHz. The loss, which at low frequencies was close to zero, becomes important at "high" (above 600 GHz) frequencies with loss tan δ = 0.006. The experimental "high frequency" phase variation bottom of Fig.24A, is close to the extrapolation at low frequency, showing a very limited dependence of the permittivity ε. The right picture shows the measured and simulated spectra of PTFE polymer, Teflon, which is commonly used for microwave lenses. A discrepancy between measured high frequency amplitude (lower amplitude trace) and the one extrapolated from lower frequency data shows that the sample becomes also lossy at higher frequencies, close to 1 THz. Transmission measurements at around 400 GHz (with extensions ASA), as demonstrated in the magnified picture of Fig. 24 below, shows that the loss increases abruptly above that frequency.

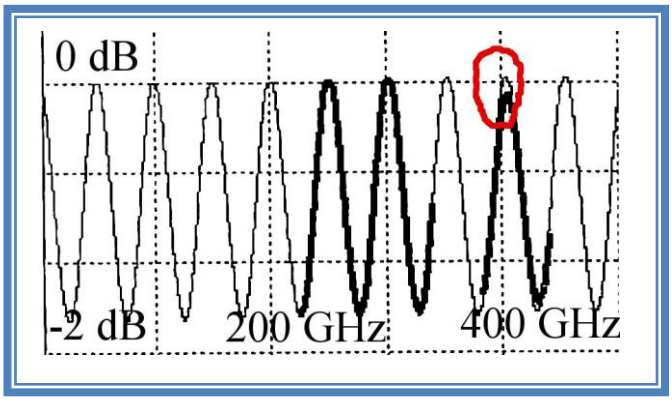

Transmission measurements of a common glass, Fig.25A, show that the loss is increasing progressively with frequency, already deviating from extrapolated 210-336 GHz behaviour (A) at 400 GHz (B1, ASA measurement), more at 500 GHz (B2, ASA measurement), and much more in the upper band (C). The Fig.25B shows a slight decrease of ε with frequency.

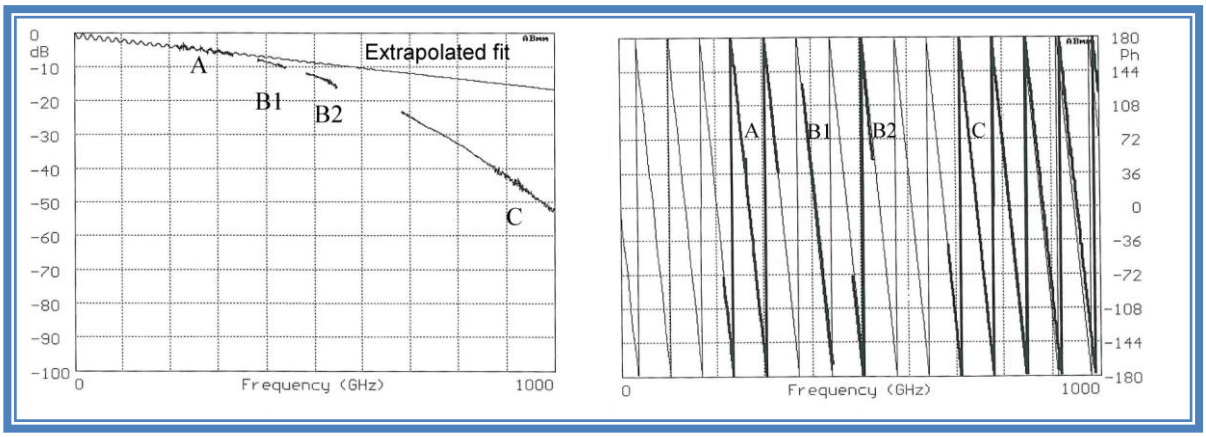

Figure 25. Spectral properties of a 4.02 mm thick glass slab at the spectral range between 0 and 1000 GHz. The left picture shows the amplitude of the transmitted signal, at several experimentally accessible spectral ranges, A, B1, B2, and C. The upper curve shows a theoretical fit of the transmission extrapolated from low frequency (data A) dielectric permittivity $\varepsilon = 4.425$ and loss tan $\delta = 0.002$. The right picture shows the phase of transmitted signal versus frequency. A slight deviation of the experimentally measured phase (thick line) from the theoretical calculations based on frequency-independent dielectric properties shows that the dielectric permittivity changes slightly with frequency above 700 GHz.

Fig.26A shows that intrinsic silicon is an ideal dielectric material up to the THz. It seems that the observed amplitude (C) is a little bit above that extrapolated from 210-336 GHz range (A). It is a very unusual dielectric behaviour in the millimeter-submillimeter domain: a loss which diminishes with frequency. The only other such case we have met was diamond. Since the measurement in the QO bench is not precise enough for the determination of small losses (there is a single crossing through the sample), we are continuing this experiment with the open cavity perturbation technique.

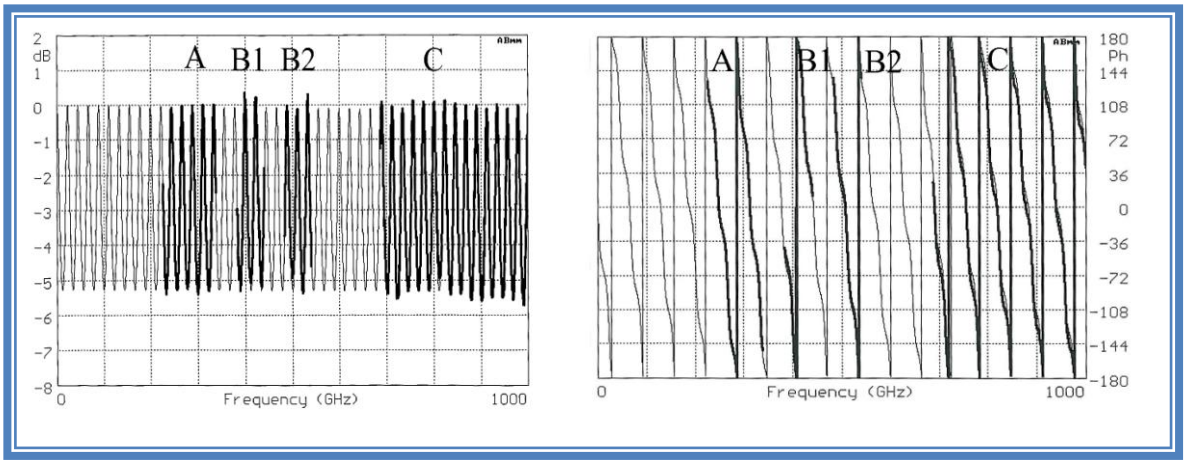

Figure 26. Transmission spectra (signal amplitude in dB on the left plot, and signal phase in degrees on the right plot) of 1.98 mm thick silicon slab. Dark lines labelled A, B1, B2, C show spectra measured over 4 bands, and light gray lines show theoretical fit. The dielectric parameters obtained from the fit are for $\varepsilon = 11.607 – 11.635$ and $\tan\delta = 0.00017 – 0.00000015$.

VI. OPEN CAVITY PERTURBATION TECHNIQUE.

VI.1. The setup.

We use a semi-spherical Fabry-Perot resonator with adjustable distance between mirrors around 15 cm. The radiation coupling is made by two irises drilled in the spherical mirror at top. The WR-8 waveguides (input/output by transmission) connected to the coupling holes are oversized for most of the frequencies used.

Figure 27. The Fabry-Perot submillimeter resonator shown together with the signal source, the detector and coupling waveguides. The sample is usually placed at the flat, bottom, mirror. Please note that the position of bottom mirror is adjustable.

The resonance is measured with the sample placed on the plane mirror. Then, the cavity resonance is remeasured without the sample, in air, and without moving the mirrors. The change of the resonance frequency corresponds to the relative permittivity of the sample, and the change of the cavity quality factor indicates the dielectric losses. The calculation of both parameters is done automatically by the MVNA software. The results presented below were obtained for the silicon sample of Fig.26.

VI.2. The "low" frequency range.

Frequencies are chosen in order to have an integer number of half-wavelengths inside the sample put on the flat mirror, so that there is no curvature of the standing wave on both sides of the sample. We have worked around 132, 155, 178, 198, 222, 332 GHz and found the following values of the dielectric constant and loss tangent: ε = 11.663 +/- 0.025, $\tan\delta$ = 4.8 (+/- 1.4) 10^{-4}, see Fig.28.

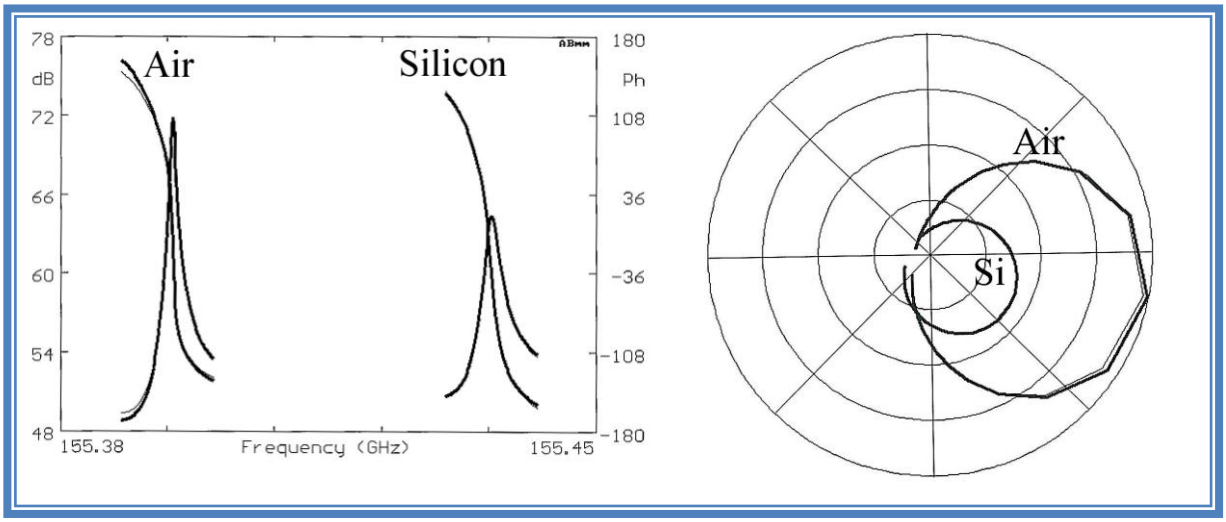

Figure 28. Example of open cavity resonances at 155 GHz with and without silicon sample. Left picture shows the amplitude (resonance) and the phase (dispersive) of the transmitted signal with the sample in the cavity, and without the sample. In the right picture both resonances and theoretical fits with Lorentz-shape curve are plotted in polar coordinates on the Smith Chart.

VI.3. The "high" frequency range.

We have worked at around 666, 821, 954 GHz and found the following material parameter values: ε = 11.753 +/- 0.03, and $\tan\delta$ = 2.6 (+/- 1.2) *10-4, see Fig.29.

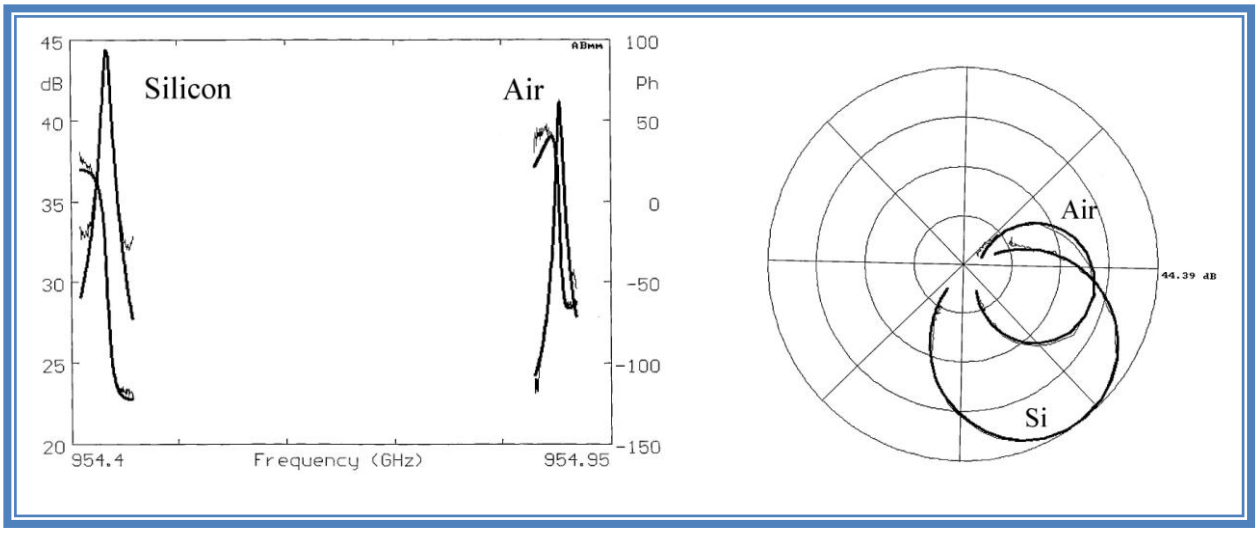

Figure 29. Example of open cavity resonances at frequency close to 1 THz with and without silicon sample. Left picture shows the amplitude (resonance) and the phase (dispersive) of the transmitted signal with the sample in the cavity, and without the sample. In the right picture both resonances and theoretical fits with Lorentz-shape curve are plotted in polar coordinates on the Smith Chart.

It seems that in pure silicon there is really a lower loss at the upper frequencies, like in diamond (which has a similar chemical structure).

VII. CONCLUSION.

The new solutions provided by AB Millimetre at WR-1.2 band covering the range 660-1000 GHz make sub-teraherz spectroscopy and diagnostics as easy to use as that at lower frequency millimeter band. Our set-up provides comprehensive access to parameter ranges and techniques already available for the WR-3.4 band 210-336 GHz (and also for the 62-112 GHz extended WR-10, W-band) both for transmission T and reflection R measurements. In fact, it is also possible to cover the whole spectral range offered by AB Millimetre for particularly demanding broad band R/T measurement, exploiting efficient and frequency independent (44-1000 GHz) quasi-optical polarizing grids diplexer (Fig. 17). That solution provides an easy to use and flexible access to the cross over teraherz spectral range.